JGR Solid Earth

RESEARCH ARTICLE
10.1029/2019JB017356

Complex Uppermost Mantle Structure and Deformation Beneath the Northwest Pacific Region

Yan Lü[1,2,4], Juan Li[1,2,4], Lijun Liu[3], and Lian-Feng Zhao[1,2,4]

[1]Key Laboratory of Earth and Planetary Physics, Institute of Geology and Geophysics, Chinese Academy of Sciences, Beijing, China, [2]Institutions of Earth Science, Chinese Academy of Sciences, Beijing, China, [3]Department of Geology, University of Illinois at Urbana-Champaign, Urbana, IL, USA, [4]University of Chinese Academy of Sciences, Beijing, China

Abstract We used a newly developed Pn tomography method to obtain high-resolution uppermost mantle velocity and anisotropy structures beneath the Northwest Pacific region. The observed Pn velocities are consistent with the local tectonic background, where high Pn velocities are observed beneath the Japan Trench area and Songliao Basin, and low Pn velocities beneath the Kuril Islands, Japan Archipelago-Izu Islands, Kyushu Island, Changbaishan-Jingpohu volcanoes, Korea Peninsula, and Japan Basin. The new Pn velocity image outlines the subducting slabs along the trenches and the young seafloor within the Japan Basin. Our results also support the existence of hot upwelling feeding the Changbaishan, Jingpohu, and Chuga-Ryong volcanoes, where small-scale mantle convection may exist below the Northeast China region. Further east, both trench-parallel anisotropy below arcs and trench-perpendicular anisotropy within the back-arc region suggest subduction-dominant mantle flow, where anisotropy may be attributable to the lattice-preferred orientation of olivine induced by flow-related strain. The highly accurate uppermost mantle velocity and anisotropy structures provide crucial information outlining the complex dynamic processes near convergent plate boundaries.

Key Points:
- We present high-resolution Pn velocity and anisotropy images in Northwest Pacific using a newly developed method
- Low Pn velocities are observed beneath Quaternary volcanoes and the young seafloor within Japan Basin
- Trench-parallel anisotropy below arcs and trench-perpendicular anisotropy within back-arc regions suggest subduction-dominant mantle flow

Correspondence to:
Y. Lü and J. Li,
lvyan@mail.iggcas.ac.cn;
juanli@mail.iggcas.ac.cn

Citation:
Lü, Y., Li, J., Liu, L., & Zhao, L.-F. (2019). Complex uppermost mantle structure and deformation beneath the Northwest Pacific region. *Journal of Geophysical Research: Solid Earth*, *124*, 6866–6879. https://doi.org/10.1029/2019JB017356

Received 12 JAN 2019
Accepted 11 JUN 2019
Accepted article online 18 JUN 2019
Published online 16 JUL 2019

1. Introduction

The Northwest Pacific region has experienced widespread tectonic deformations during the Cenozoic as a result of complex plate interactions in the region. The Pacific and Philippine Sea plates are subducting beneath the Okhotsk and Eurasian plates, resulting in the marginal seas, continental rift zones, and wide distributed island arcs (Metcalfe, 2006; Northrup et al., 1995; Ren et al., 2002; Zhao, 2017), where earthquakes and volcanic eruptions occur frequently. It is an ideal and important area for investigation of the underlying geodynamic processes of plate interactions (Figure 1). Tomographic studies have revealed that the Pacific Plate subducts from the Japan trench to the mantle and then rests in the upper mantle transition zone, with the leading edge reaching the interior of China (Fukao et al., 1992; Huang & Zhao, 2006; Lei & Zhao, 2005; Li et al., 2008; Li et al., 2013; L. Zhao et al., 2012; Zhao et al., 2013). The subduction and dehydration of the Pacific plate caused a series of volcanoes in the Japanese island arc. Recent works also proposed the existence of hot mantle upwelling below Northeast China (Guo et al., 2016; Huang & Zhao, 2006; Li et al., 2008; Li et al., 2017; Liu et al., 2017; Shen et al., 2016; Tang et al., 2014; Wei et al., 2015; Zhang et al., 2013; Zhao et al., 2015; Zhou & Lei, 2016). However, due to the limitation of data and methods, published imaging results still lack consensus. For example, the seismic structures beneath the Changbai volcano are debated, where both slow (Tang et al., 2014; Wei et al., 2015; Zhou & Lei, 2016) and fast (Sun & Kennett, 2016) *P* wave velocity of the uppermost mantle are proposed; Pn velocities beneath the Songliao Basin and Korea Peninsula also differ (Sun & Kennett, 2016; Zhou & Lei, 2016). In addition, the insufficient ray coverage has resulted in ambiguous images beneath the Japan Sea area (Legendre et al., 2015; Pandey et al., 2014; Schaeffer & Lebedev, 2013; Takeuchi et al., 2014; Wei et al., 2015). Therefore, it is challenging to understand the geodynamic characteristics of the Northwest Pacific region. Here we attempt to better address this problem using Pn velocity and anisotropy tomography with an improved methodology.

The Pn wave travels along the topmost mantle and can be used as the dominant and most sensitive phase to constrain the velocity and anisotropy structure beneath the Moho. Variations of Pn wave velocity reflect the internal thermal state around the Moho depth and can be used to reveal the properties of the shallow mantle material (Hearn et al., 2004; Pei et al., 2007, 2011; Wang et al., 2013). Upper mantle anisotropy is generally considered a result of mantle flow-induced lattice-preferred orientation (Kaminski & Ribe, 2001; Zhang &

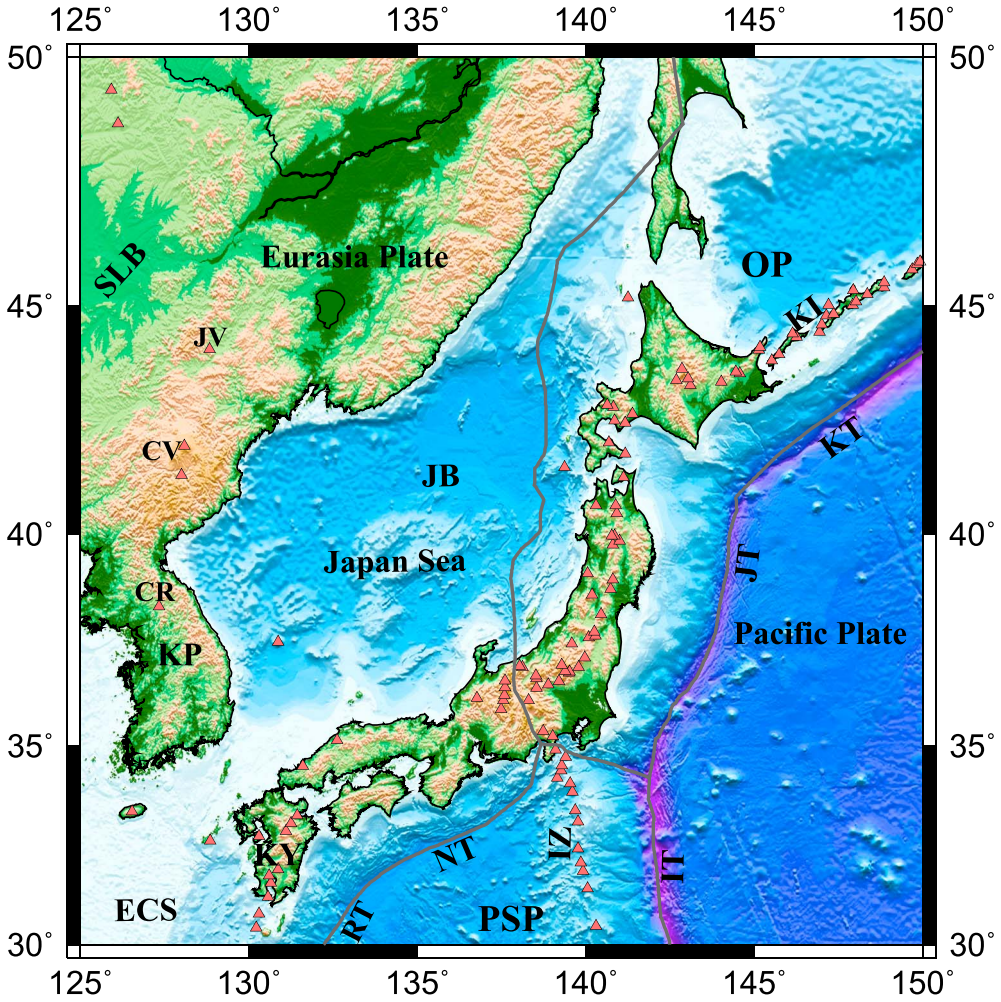

Figure 1. Simplified tectonic map of the study area. CR = Chuga-Ryong volcano; CV = Changbaishan volcano; ECS = East China Sea; IT = Izu-Bonin Trench; IZ = Izu Islands; JB = Japan Basin; JT = Japan Trench; JV = Jingpohu volcano; KI = Kuril Islands; KP = Korea Peninsula; KT = Kuril Trench; KY = Kyushu Island; NT = Nankai Trough; OP = Okhotsk Plate; PSP = Philippines Sea Plate; RT = Ryukyu Trench; SLB = Songliao Basin. Triangles denote Quaternary volcanoes, and gray lines denote plate boundaries. Background colors represent topography.

Karato, 1995). Proposed tectonic origins for anisotropy under the upper plate include absolute plate motion (e.g., Fouch et al., 2000) and subduction-induced mantle flow (e.g., Hu et al., 2017; Long, 2013). Pn wave anisotropy can reflect orientation of peridotite crystals in the uppermost mantle and provide information about the deviatoric stress field (Karato & Jung, 1998; Ribe, 1992). Thus, a good image of Pn velocity and anisotropy in the uppermost mantle is of great help for understanding the thermal state of the mantle and related dynamic processes. Recently, we improved the accuracy of the Pn velocity and anisotropic inversion method by considering the variation of crustal thickness (Lü et al., 2017). The increasing quality and quantity of seismic data in the Northwest Pacific has enabled a good coverage of Pn rays in the Japan Sea and Northeast China. We applied the newly developed method and obtained a high-resolution Pn velocity and anisotropy map, which provides an improved seismological basis for studying plate subduction and mantle dynamics, as well as the mantle structure below the volcanic zone and back-arc basins.

2. Data and Method

2.1. Data

The study area is located at 30–50°N and 125–150°E. The Pn data we used are from the ISC-EHB catalog of International Seismological Centre (1960–2013) and the China National Seismic Network (1990–2017). To

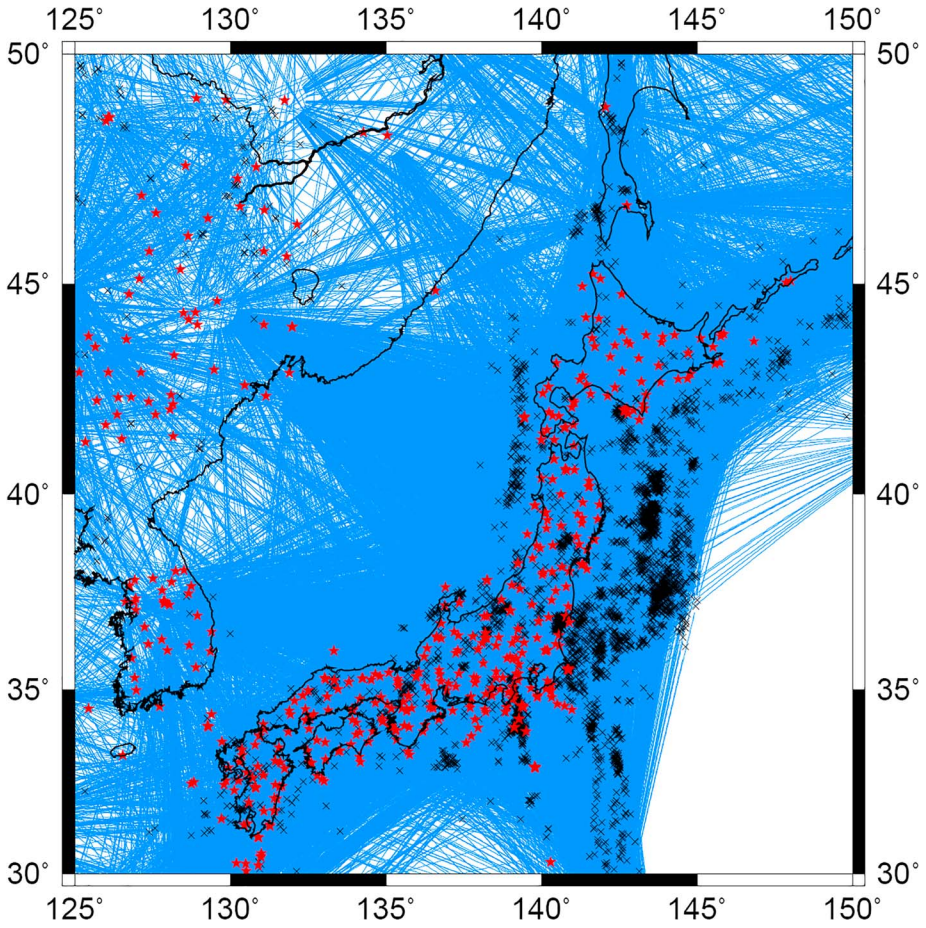

Figure 2. Events, stations, and raypaths for Pn travel times used in this study. Events are represented by black crosses, and stations are denoted by red stars.

ensure the data quality, the following criteria were used: epicentral distances are between 2° and 12°; each station has at least five Pn records, and each event is recorded by at least five stations; the event depth is above the Moho given in the CRUST 1.0 model (Laske et al., 2013); travel time residuals are limited to a range of ±5 s. In total, 191,649 seismic data from 11,606 events recorded by 1,156 stations within 20–60°N and 115–160°E were used in this study (Figure 2).

2.2. Method

The Pn tomography method was first developed by Hearn (1984, 1996). The uppermost layer of mantle is divided into a set of two-dimensional cells in which the slowness (the inverse of velocity) of the cell is to be inverted. To reduce the errors caused by the Moho depth variation, we proposed a modified Pn velocity and anisotropy tomography method by considering the Moho depth variation using the CRUST 1.0 model (Lü et al., 2017).

For a Pn ray traveling from the event to the uppermost mantle,

$$\Delta T_{in} = \frac{\Delta b_{in}}{v_c} - \frac{\Delta h_{in} \cdot tan\ \alpha}{v_m} = (h_{in} - h_{ave}) \cdot \sqrt{\frac{1}{v_c^2} - \frac{1}{v_m^2}}, \quad (1)$$

where Δh_{in} is the change in Moho depth at the entrance point, ΔT_{in} is the change in travel time by Δh_{in}, Δb_{in} is the change in travel distance in the crust of the entrance raypath, α is the entrance angle, v_c is the average crustal velocity, v_m is the average uppermost mantle velocity, h_{in} is the Moho depth at entrance point of the ray, and h_{ave} is the average Moho depth.

Similarly, for the Pn ray traveling from the uppermost mantle to station

$$\Delta T_{out} = (h_{out} - h_{ave}) \cdot \sqrt{\frac{1}{v_c^2} - \frac{1}{v_m^2}} \tag{2}$$

thus, for the Pn ray

$$\Delta T = \Delta T_{in} + \Delta T_{out} = (h_{in} + h_{out} - 2h_{ave}) \cdot \sqrt{\frac{1}{v_c^2} - \frac{1}{v_m^2}} \tag{3}$$

where ΔT is the change in travel time by the Moho depth variation for the Pn ray, ΔT_{out} is the change in travel time by Moho depth variation at the exit point of the ray, and h_{out} is the Moho depth at the exit point.

Then, the modified Pn travel time residuals can be described approximately by the perturbation equation

$$T_{ij} - \Delta T_{ij} = a_i + b_j + \sum_k d_{ijk} \cdot \left(S_k + A_k \cos 2\phi_{ijk} + B_k \sin 2\phi_{ijk} \right) \tag{4}$$

where T_{ij} is the travel time residual for event j at station i, ΔT_{ij} is the Moho depth correction for the ray ij, a_i is the static delay for station i, b_j is the static delay for event j, d_{ijk} is the travel distance of ray ij in mantle cell k, S_k is the slowness perturbation for cell k, A_k and B_k are the anisotropy coefficients for cell k, and ϕ_{ijk} is the back azimuth angle of the ray ij in cell k. The magnitude of the anisotropy is given by $\sqrt{A_k^2 + B_k^2}$, and the direction of the fastest wave propagation is given by $90^\circ + \frac{1}{2} \arctan \frac{B_k}{A_k}$ (Pei et al., 2007), where the arctangent function is evaluated to lie between –180° and +180° depending on the signs of A_k and B_k. The unknown parameters in equation (4) are the mantle slowness perturbation S_k, the anisotropy parameters A_k and B_k, and the station and event delays a_i and b_j, respectively. The set of equation is solved by the LSQR algorithm (Paige & Saunders, 1982). Two damping constants are applied to the unknown slowness and anisotropy coefficients, respectively, and damping is not considered for the station or event terms.

In this study, the cell size is set as $20' \times 20'$. Two-hundred iterations of inversion are conducted with a constant damping value of 500 for both velocity and anisotropy parameters, chosen by the trade-off analysis of velocity variation and travel time fitting. The standard deviation of residual decreased from 1.9 to 0.8 s during the inversion (Figure 3).

2.3. Resolution Test

Checkerboard tests were conducted to determine the size of features that can be reliably imaged and interpreted. The checkerboard test was created by assigning both sinusoidal velocity and anisotropy anomalies to the model cells. The average amplitudes ($\max\Delta v/\sqrt{2}$) of the sinusoidal velocity and anisotropy were 0.3 and 0.15 km/s, respectively. Synthetic arrival times were calculated for the test model for different checkerboard sizes with the same distribution of earthquakes, stations, and raypaths as those used in the tomographic inversion of the real data. Gaussian noise with a standard deviation of 0.8 s, which is comparable to the root mean square residuals after inversion, was added to the synthetic travel times. The tests indicate that for most of the study region, $1.5^\circ \times 1.5^\circ$ cells can be resolved well for the Pn velocity (Figure 4a). The spatial resolution of velocity in regions with high ray coverage can reach $1.0^\circ \times 1.0^\circ$ or better. The resolution for the anisotropy model can reach $2.5^\circ \times 2.5^\circ$ or better in regions with high ray coverage (Figure 4b). In the areas where the raypath coverage is poor or the raypath direction are not equally distributed, the anisotropy inversion results may be affected by the different travel depths of different travel distances. Nevertheless, the high dense raypath coverage and the strong true Pn anisotropy structure can overcome the noise caused by this. Therefore, in this study, we only discuss the strong signatures of the anisotropy model.

2.4. Station and Event Delays

The station delay and event delay parameters were used to absorb the travel time delay due to errors in the crustal model and event locations. The station delays in our study (Figure 5a) are primarily related to the differences between the CRUST 1.0 model and the real earth. For example, positive station delays indicate the crust beneath the stations are thicker or has lower seismic velocity than that in CRUST 1.0. The conformity of the station and event delay patterns indicates the good quality of the inversion. In addition, the event

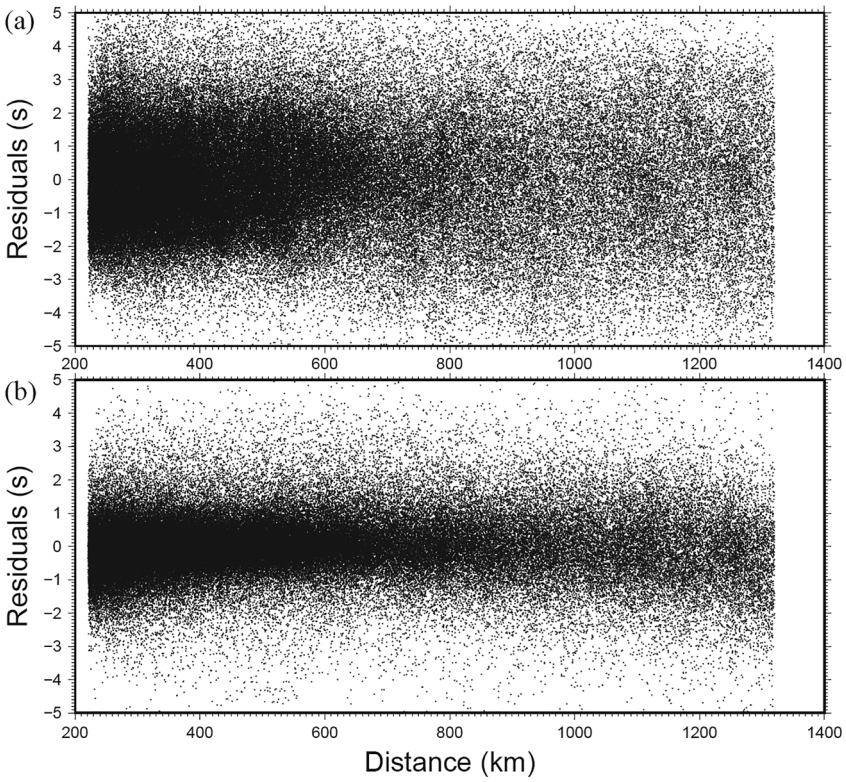

Figure 3. Distribution of Pn travel time residuals versus epicentral distance (a) before and (b) after inversion.

delay items (Figure 5b) also reflect errors in the earthquake location or focal depth and are therefore larger than the station delay.

3. Results

The average Pn velocity is 8.02 km/s in the study area, and the velocity perturbations are approximately ±4% (Figure 6). In general, high Pn velocities are distributed beneath the Japan Trench area and Songliao Basin,

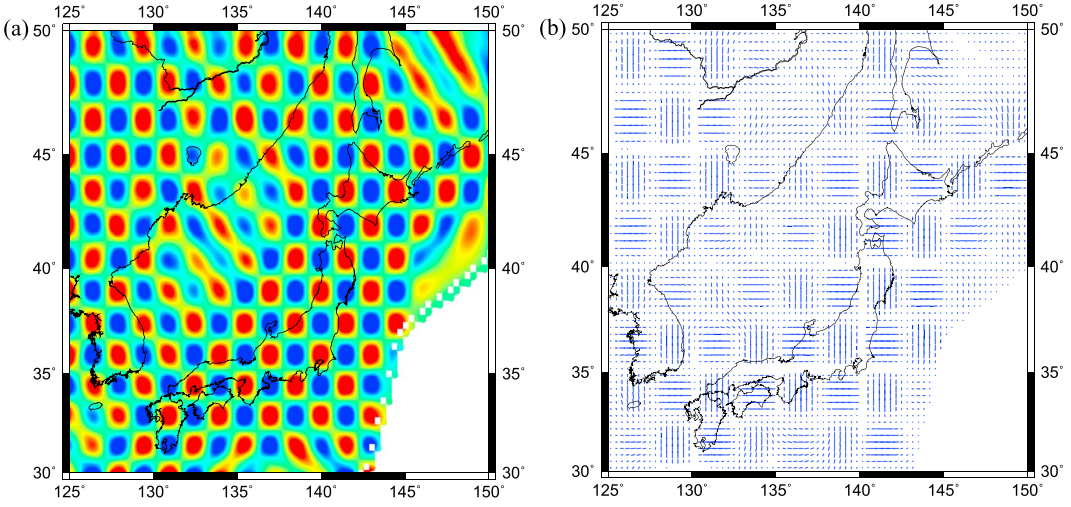

Figure 4. The checkerboard resolution test results for (a) velocity and (b) anisotropy of the study area. The sinusoidal velocity and anisotropy checkerboard sizes are (a) 1.5° × 1.5° and (b) 2.5° × 2.5°.

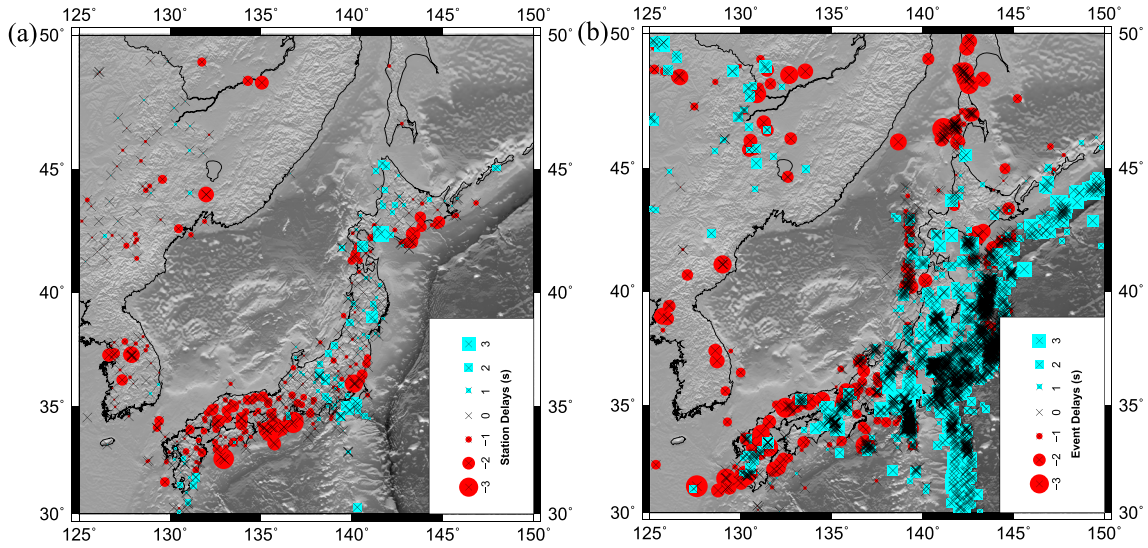

Figure 5. Station delays (a) and event delays (b) for Pn travel times of the study area. Crosses represent stations and events. Red circles indicate early arrival times, and cyan squares indicate late arrival times, with sizes proportional to the delay time.

while low Pn velocities are distributed mostly beneath volcanic arcs, the Kuril Islands-Japan Archipelago-Izu Islands, Kyushu Island, and the intraplate Changbaishan-Jingpohu volcanoes, Japan Basin, and part of Korea Peninsula as well.

Figure 7 shows the tomographic image of the Pn velocity and anisotropy in the study area, where several regions with significant Pn anisotropy and good ray coverage are outlined. The volcanic arcs demonstrate distinct anisotropy patterns from regions further inland. At the western of Kuril Trench, Nankai Trough, and Ryukyu Trench (regions A, B, D, and E), the fast Pn directions generally along the NE-SW direction. At the western of Japan Trench and Izu Trench, the fast Pn direction is mostly N-S (regions C and F). These directions are largely parallel to the trench. In contrast, the back-arc regions demonstrate clear trench-normal Pn anisotropy. For example, regions in the northwest Japan Archipelago (G, I, and J) have a generally NW-SE fast orientation, and region H has an E-W orientation, both perpendicular to the trench segment nearby.

4. Discussion

In general, high Pn velocities indicate stable lithospheric structures and low temperatures, whereas low Pn velocities indicate either elevated temperatures in the uppermost mantle or the presence of chemically modified regions (Hearn, 1999; Karato & Jung, 1998). In addition, low Pn velocities beneath volcanoes can indicate hot mantle upwelling. Pn anisotropy in the uppermost mantle is commonly thought to be associated with the preferred alignment of olivine crystals and can reflect the stress state in the uppermost mantle and indicate the deformation pattern along the collision boundary (Hearn, 1999; Ribe, 1992). Due to the limitation of data and method, previous Pn tomography studies (Li et al., 2017; Sun & Kennett, 2016; Wang et al., 2013; Zhou & Lei, 2016) mostly focus on velocity, with little effort on resolving anisotropy beneath this region. The newly developed method and denser data coverage in this study provide an unprecedented opportunity to simultaneously obtain a more accurate Pn velocity and anisotropy structure than before. In the following, we will discuss the major features of Pn velocity and anisotropy and their associated tectonic implications.

4.1. Kuril Islands-Japanese Archipelago

Velocity structure beneath this region has been investigated by many seismic tomography studies (Li et al., 2008; D. Zhao et al., 2012, Zhao et al., 2013, 2016; Wang et al., 2013; Wang & Zhao, 2013; Takeuchi et al., 2014; Asamori & Zhao, 2015; Legendre et al., 2015; Wei et al., 2015; Liu & Zhao, 2016; Niu et al., 2016; Sun & Kennett, 2016; Zhou & Lei, 2016; Li, Song, & Li, 2017; Zhang et al., 2019). The Pacific lithosphere

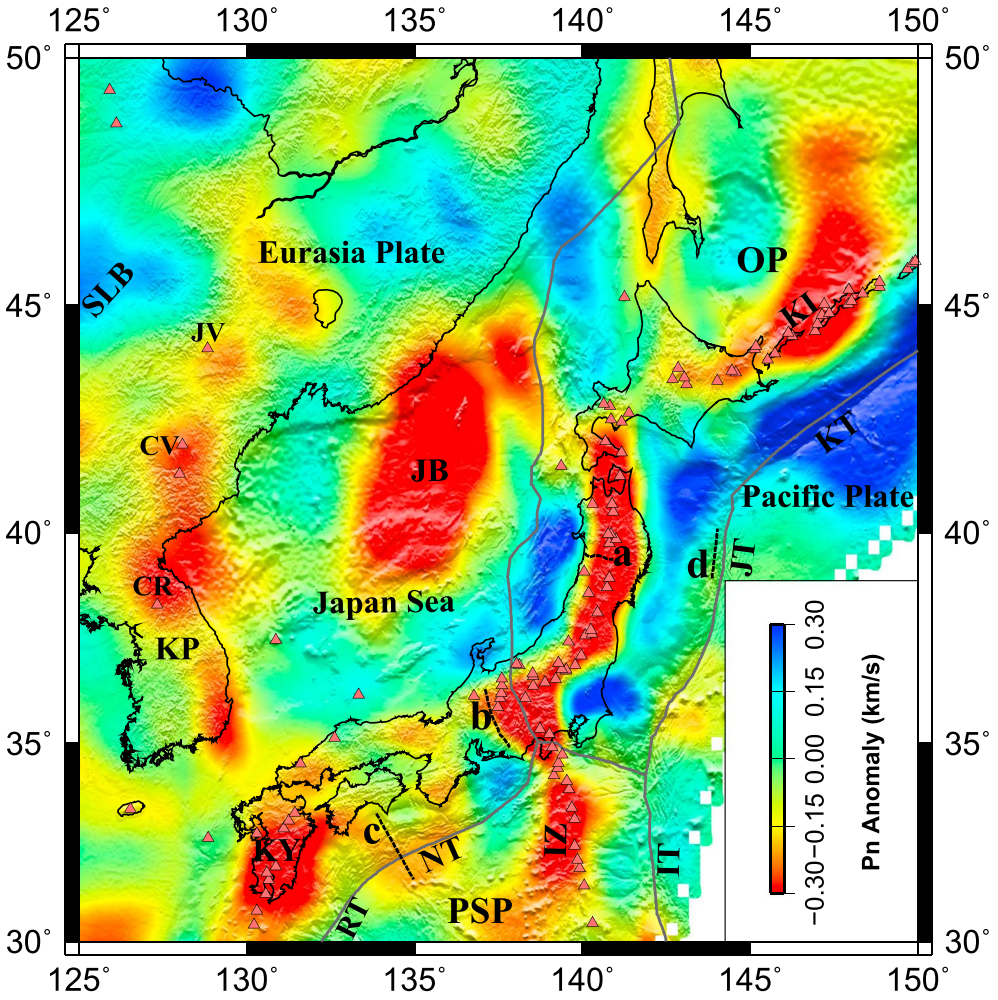

Figure 6. Pn lateral velocity variations in the study area. Red areas correspond to low velocity, and blue areas correspond to high velocity. Triangles denote Quaternary volcanoes, and gray lines denote plate boundaries. Dashed black lines marked a, b, c, and d denote four profile lines, respectively.

has been imaged as a high-velocity slab subducting beneath the Eurasia Plate. Low seismic velocities are also found beneath the Japan Islands and volcanoes. In the new high-resolution images we obtained, the high Pn velocity anomaly adjacent to the Kuril-Japan trench confirms the cold subducting Pacific lithosphere. Both the location and orientation of prominent low Pn velocity patches are consistent with the distribution of island volcanoes, implying a hot mantle wedge with possible material upwelling above the downgoing Pacific slab beneath these island arcs. The upper mantle *P* velocity model by Zhao et al. (2013) and Liu and Zhao (2016) revealed a similar low-velocity structure around the Japan trench at the Moho depth. Asamori and Zhao (2015) published a shear velocity model obtained from teleseismic tomography, and their *S* wave velocity structure at depth of 40 km is very similar to our Pn velocity image; the main difference is the *S* wave velocity in their model is not low beneath the Izu Islands and volcanoes, and we argue that the low ray coverage of their study at Izu is the reason.

Our Pn image is also consistent with seismic refraction and reflection surveys conducted beneath Japan Islands. The uppermost mantle *P* velocity has a value of 7.6–7.7 and 7.6–7.9 km/s beneath profiles a and b, respectively (Figure 6; Iwasaki et al., 2001; Iidaka et al., 2003). The low velocities imaged in both regions correspond well to the high volcanic activity since 10–15 Ma, indicating the existence of hot upwelling material from the depth greater than the Moho. The profile c crosses the Nankai Trough, and the Pn velocity is ~7.8 km/s (Kodaira et al., 2000), which is consistent with our study. Another profile d is located adjacent to the Japan trench, with the striking direction roughly parallel to the trench. The Vp velocity from

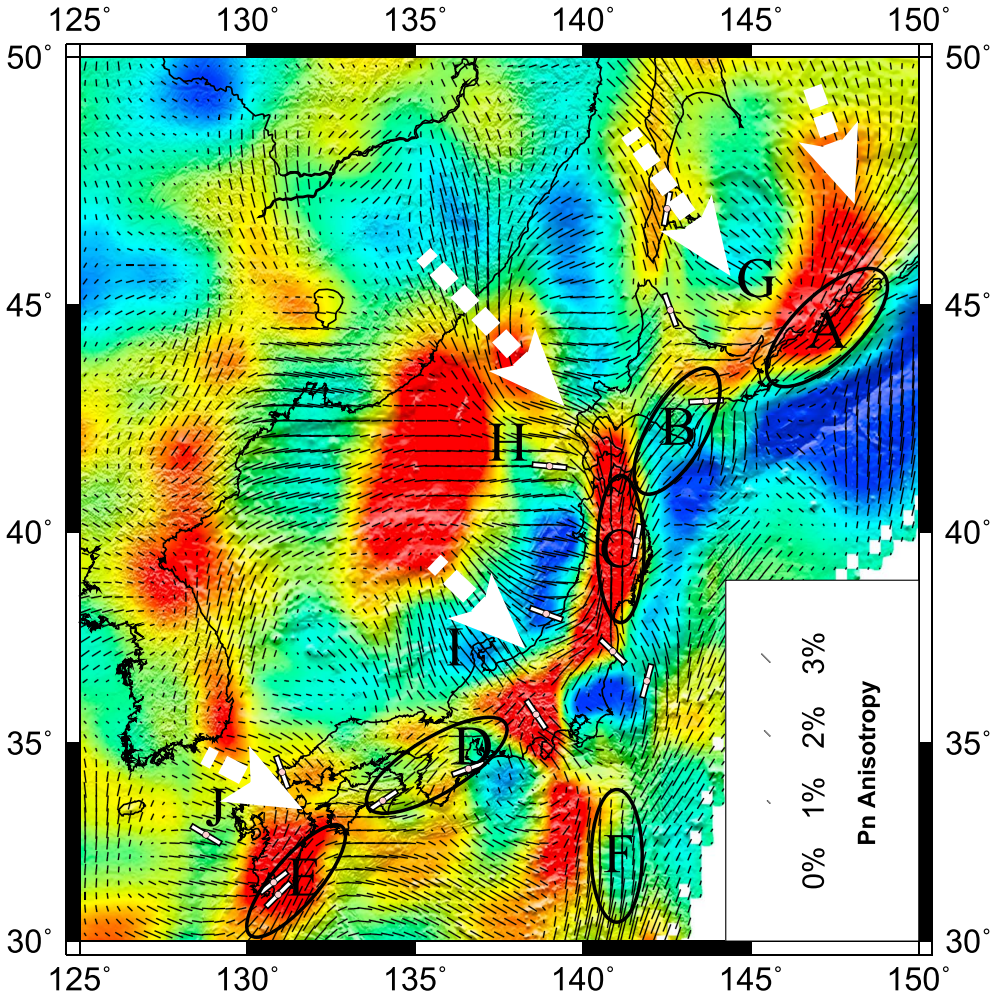

Figure 7. Tomographic image of the Pn velocity and anisotropy in the study area. The velocity color bar is the same as in Figure 6. Short black bars represent the fast direction of the anisotropy with their lengths proportional to the magnitude of anisotropy. Regions exhibiting large anisotropy and having dense ray coverage are outlined with black ovals. Thick dashed white arrow lines mark inferred regional mantle flow direction above the slab. The white bars with a pink core indicate the fast direction measured from previous shear-wave splitting studies (Long & van der Hilst, 2005; Nakajima et al., 2006).

refraction seismic analysis is ~8.0 km/s (Azuma et al., 2018), almost the same value as our Pn image. Since the seismic refraction and reflection surveys are the most accurate in seismological methods; therefore, the consistency between our model and the active seismic profiles proves that our high-resolution Pn model is reliable.

The Pn anisotropy sheds new light on the dynamic evolution of the region. For example, the fast Pn directions above the Pacific and Philippine Sea subduction zones are remarkably parallel to the collision boundaries (Figure 7, regions A–F). The boundary-parallel anisotropy structure had been observed at collisional boundaries by other researchers (Cai et al., 2018; Hearn, 1999; Huang et al., 2015; Long, 2013; Lü et al., 2012, 2017; Wang & Zhao, 2013; Wei et al., 2015). This anisotropy pattern can be explained by the dominance of B-type olivine due to water enrichment beneath the active arc volcanoes. The B-type anisotropy forms in olivine in the presence of water; unlike normal mantle anisotropy, the fast direction forms perpendicular to the direction of shearing, thus forming arc-parallel anisotropy. Further west and northwest to the Japan Archipelago, the fast direction of Pn anisotropy is overall perpendicular to the closest trench segment (Figure 7, white arrow lines near regions G–J). This trench-perpendicular fast direction can be explained by the lattice-preferred orientation of olivine induced by flow-related strain (Nakajima et al., 2006; Nakajima & Hasegawa, 2004; Zhao, 2017). We plot the shear-wave splitting measurements of category I

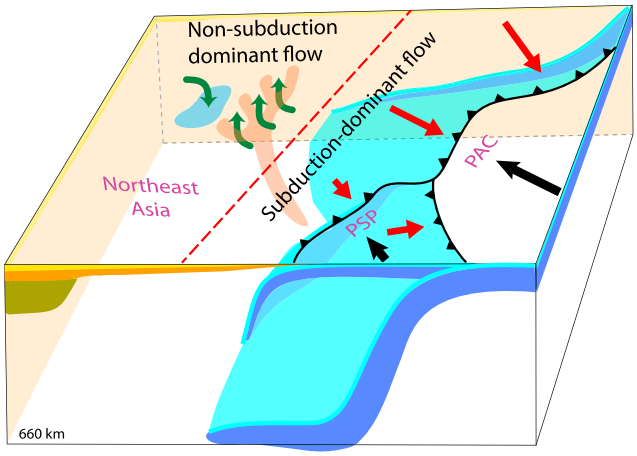

Figure 8. A sketch showing the tectonic components and mantle dynamic processes below Northwest Pacific. PAC=Pacific Plate; PSP=Philippines Sea Plate. Bold black arrows represent plate motion, bold red arrows indicate horizontal mantle flow, and green bold arrows indicate vertical mantle flow. The cyan/blue colors outline slabs.

with high quality in Long and van der Hilst (2005) and the regional average shear-wave splitting by Nakajima et al. (2006) in Figure 7. The fast directions of the shear wave agree well with the Pn fast direction near the collision boundary. Boundary-parallel shear-wave splitting fast direction below arcs (C–E) and trench-perpendicular fast direction within back-arc regions (H–J) are observed. These observations indicate that the subduction-dominant mantle flow is the primary cause for the observed seismic anisotropy pattern beneath this region.

A recent geodynamic modeling study suggests that the regional-scale pattern of trench-perpendicular anisotropy in South America reflects the dominant control on mantle flow from the subducting Nazca slab (Hu et al., 2017). The Pacific subduction closely resembles the Nazca plate, in their fast subduction rate, large trench width, and concaved geometry of the subduction zone. We therefore suggest that the observed anisotropy in our study region also reflects a subduction-dominant mantle flow field with an overall converging pattern toward the trench (Figure 7), similar to that below South America (Hu et al., 2017). In comparison to the global anisotropy model used in South America (Hu et al., 2017), our regional results clearly resolve more flow features (Figure 7). These include the local variations of flow structure associated with the abrupt changes of trench curvature: The curving Pacific trench seems to induce local variations of the anisotropy orientation, where the patterns next to the sharpest kinks (H & I in Figure 7) display apparent transitions from nearby trench segment. In addition, the flow associated with the Pacific slab appears stronger than that with the Philippine Sea slab, as can be seen from larger anisotropy amplitude and more spatially extensive anisotropy patterns in the north-central part of the region (Figure 7). This is physically consistent with the faster subduction speed and, thus, stronger trench-ward poloidal flow above the Pacific slab. Combining our new inversion model, previous 3-D tomography models, and current geodynamic understanding on subduction and mantle flow, we summarize the plausible tectonic components and mantle dynamic processes below Northwest Pacific in Figure 8.

4.2. Northeast China-Korea Peninsula

Further inland in our study region, it is suggested that there is an upper mantle upwelling beneath the Changbaishan volcano (Huang & Zhao, 2006; Lei & Zhao, 2005; Li et al., 2012; Takeuchi et al., 2014; Tang et al., 2014; Wei et al., 2015). Some high velocities at mantle depth are observed beneath the Songliao Basin (Guo et al., 2016; Huang & Zhao, 2006; Li et al., 2012; Liu et al., 2017; Sun & Kennett, 2016; Xin et al., 2018; Zheng et al., 2011). Built upon the *S* wave velocity imaging, Guo et al. (2016) propose a mantle convection model for Northeast China. Liu et al. (2017) observed low-velocity anomalies in the upper mantle beneath the Jingpohu volcano using ambient noise adjoint tomography. However, due to the limited data and methods, previous Pn studies had different results for this area. Both slow (Zhou & Lei, 2016) and fast (Sun & Kennett, 2016) Pn velocities are obtained beneath the Changbaishan volcano, and Pn velocities beneath the Songliao Basin and Korea Peninsula also differ (Sun & Kennett, 2016; Zhou & Lei, 2016).

With the new method and more data, we obtained a more detailed Pn structure beneath this region. In our study, low Pn velocities are observed beneath the Changbaishan volcano, Jingpohu volcano, and the Korea Peninsula, and relatively high Pn velocities are found beneath the Songliao Basin. Although the Songliao Basin is an extended basin, we consider that the high Pn velocity may be caused by some downwelling due to small-scale mantle convection below the region. Our Pn model also suggests that upper mantle hot upwelling processes feed the Changbaishan, Jingpohu, and Chuga-Ryong volcanoes. The separate low Pn velocities beneath the Changbaishan volcano and Jingpohu volcano indicate that, even if the hot upwelling beneath the volcanoes may be originally from the same deeper source, they are separate in the uppermost mantle.

The Pn anisotropy in this region demonstrates a different pattern from that further east. Although the fast anisotropy orientation related to Pacific subduction seems to extend into Northeast China to the north of

45°N, this continuity of anisotropy structure clearly breaks down further south, where recent intraplate volcanoes outlined by low-velocity anomalies mark a distinct transition of anisotropy pattern from that associated with subduction on the east (Figure 7). Huang et al. (2014) revealed a similar *P* wave anisotropy pattern of uppermost mantle on both sides of the 45°N in Northeast China. This observation implies a different pattern of mantle flow below Northeast China from that to the east. Relevant geodynamic features for the region include a single upper-mantle upwelling beneath the Changbaishan volcano (Tang et al., 2014), isolated slow anomalies at the uppermost mantle (Figure 6), and cold downwelling beneath the Songliao Basin (Guo et al., 2016). Collectively, we interpret that the different low anomalies at the uppermost mantle depth associated with the active volcanoes (Figure 6) likely all originate from the same upper-mantle upwelling (Tang et al., 2014) and that these imaged high and low anomalies under Northeast China are density anomalies that drives the local convection (Figure 8).

4.3. Japan Sea

The Japan Sea is an important part of the western Pacific trench-arc-basin composite system and belongs to a typical back-arc sea. It is a key area for studying the subduction dynamics of the northwest Pacific and the evolution of the back-arc basin. Studies have revealed a very thin crust and high Bouguer gravity anomalies beneath the Japan Basin (Wang et al., 1999; Watts & Bodine, 1978). Based on a combination of bottom sampling data, geomagnetic data, and seismic refraction and reflection survey, it is confirmed that there are typical oceanic crusts in the Japan Basin and continental or transitional crusts at the southern part of the Japan Sea (Hirata et al., 1992; Horne et al., 2017; Jolivet et al., 1994; Xu et al., 2014; Yoon et al., 2014). However, due to the lack of stations and earthquakes within the region, previous travel-time tomography studies only revealed low resolution and large-scale low-velocity anomalies in the upper mantle beneath the Japan Sea (Legendre et al., 2015; Pandey et al., 2014; Schaeffer & Lebedev, 2013; Takeuchi et al., 2014; Wei et al., 2015), making it difficult to effectively infer the details of oceanic crust development in the Japan Sea. Due to the unique propagation path of Pn waves, the use of abundant stations and earthquakes around the Japan Sea results in a dense Pn-wave ray coverage of the uppermost mantle below the Japan Sea, where the traditional travel time inversion is less capable to resolve. Our Pn velocity imaging reveals a large patch of low velocity anomaly just beneath the Japan Basin, whose spatial extent is consistent with the oceanic crust distribution (Horne et al., 2017; Watts & Bodine, 1978). From our high-resolution image, we also found that the Pn velocity beneath the other areas of the Japan Sea is not as low as the Japan Basin. The large-scale low velocity beneath the whole Japan Sea in previous tomography studies may be due to low-density ray coverage and the low seismic resolution beneath the Japan Sea area. Our study thus provides new tomographic evidence of the lithospheric heterogeneity beneath the Japan Sea.

The distribution of temperature and seismic velocity within young oceanic lithosphere represents an outstanding scientific question. Nishimura and Forsyth (1989) conducted a basic study on the seismic velocity variation of Rayleigh wave and Love wave on both sides of the mid-ocean ridge and found that the surface wave velocity increases with age on both sides of the mid-ocean ridge. More recent surface wave imaging studies found that the surface wave velocity of ~20-Ma lithosphere is about 5% lower than global average (Yao et al., 2011; Zhou et al., 2006). Due to the lack of seismic station distribution on the flanks of the mid-ocean ridge, high-resolution mantle *P* wave imaging results are lacking in the past. The Japan Basin was the center of postarc extension occurred at ~30–15 Ma, during which the oceanic crust of the Japan Basin was produced (Wang et al., 1999; Xu et al., 2014). In this Pn study, our results show that the *P* wave velocity of uppermost mantle below young ocean crust of ~15–30 Ma age is 4–5% lower than normal. It provides a new seismological basis for studying seismic wave velocity variation on both sides of the mid-ocean ridge. The spread direction of Japan Basin was N-S at ~30–15 Ma (Hirata et al., 1992; Jolivet et al., 1994; Xu et al., 2014). The present E-W fast Pn direction beneath the Japan Basin indicates the lattice-preferred orientation of olivine was rearranged by the subduction-induced mantle flow since then.

5. Conclusions

Our high-resolution uppermost mantle Pn velocity and anisotropy measurements beneath the Northwest Pacific region provide new insights on the complex mantle structures and dynamic processes. The observed Pn velocities are consistent with the local tectonic background, including the high velocities beneath Japan Trench and Songliao Basin, and low Pn velocities beneath the Kuril Islands, Japan Archipelago-Izu Islands,

Kyushu Island, Changbaishan-Jingpohu volcanoes, Korea Peninsula, and Japan Basin. Our new Pn velocity image outlines the subducting slabs along the trenches and the young seafloor within the Japan Basin. The result also supports the existence of hot upwelling feeding the Changbaishan, Jingpohu, and Chuga-Ryong volcanoes, where small-scale mantle convection may exist underneath. This 3-D mantle dynamics is further confirmed by Pn anisotropy, where an E-W contrast of mantle flow patterns is observed: Both boundary-parallel anisotropy below arcs and trench-perpendicular anisotropy within the back-arc regions suggest subduction-dominant mantle flow, and the distinct anisotropy pattern below Northeast China implies a different flow regime, possibly due to local convection below the volcanoes and basins.

Appendix A: Comparison With Isotropic Inversion

To show the effectiveness of the anisotropy tomography, we also obtained the isotropic velocity model following equation (A1) with the same parameters as those in the anisotropic Pn tomography.

$$T_{ij} - \Delta T_{ij} = a_i + b_j + \sum_k d_{ijk} \cdot S_k \tag{A1}$$

The isotropic velocity model (Figure A1) has similar major patterns with the anisotropic model. High velocities are observed beneath the Japan Trench area and Songliao Basin, whereas low velocities are found

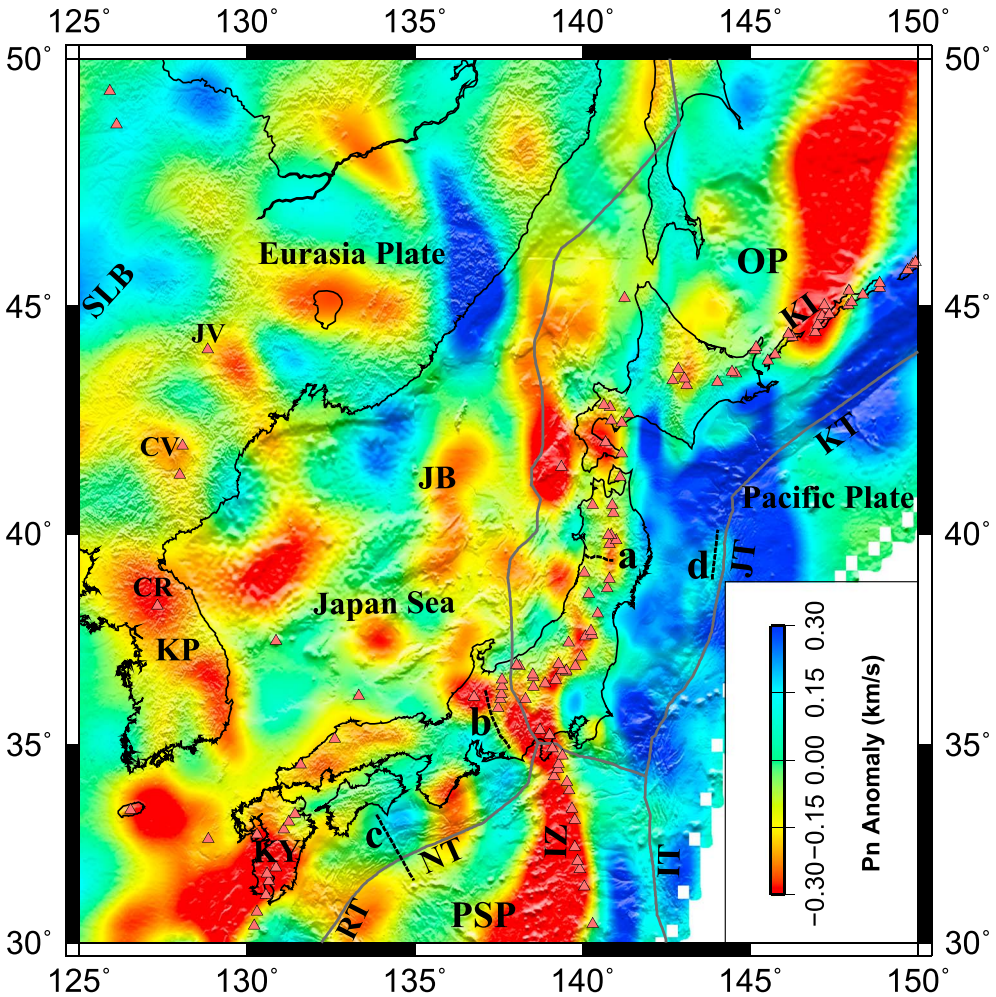

Figure A1. Isotropic Pn velocity inversion results in the study area. Red areas correspond to low velocity, and blue areas correspond to high velocity. Triangles denote Quaternary volcanoes, and gray lines denote plate boundaries. Dashed black lines marked a, b, c and d denote four profile lines, respectively.

beneath the Japan Archipelago, Japan Sea, Changbaishan-Jingpohu volcanoes, and Korea Peninsula regions. The main differences include the following: (1) The low Pn velocities beneath Honshu in the isotropic model is not as prominent, and (2) the low velocities beneath the north Japan Sea is not as continuous as that in the anisotropy model. These differences are attributed to the strong anisotropy beneath these regions. In addition, compared with the results from seismic refraction and reflection surveys beneath profiles a–c, the isotropic model shows less consistency than the anisotropic model. Therefore, we believe, with the high-density raypath coverage, the two-dimensional Pn tomography method can provide a high-accuracy seismic velocity and anisotropy structure of the uppermost mantle.

Acknowledgments
The travel time data used in this study are from the International Seismological Centre (2016, https://doi.org/10.31905/D808B830) and the China Earthquake Datacenter (http://data.earthquake.cn) of China National Seismic Network (2007, https://doi.org/10.11998/SeisDmc/SN). The CRUST 1.0 model data were downloaded from the Institute of Geophysics and Planetary Physics website (http://igppweb.ucsd.edu/~gabi/rem.html). Most Figures were prepared using the Generic Mapping Tools (Wessel et al., 2013). The anisotropic Pn model of this study is available online (doi: 10.5281/zenodo.2611077). We thank Prof. Wenliang Xu and Walter Mooney for the helpful discussions. We are grateful to the reviewer Prof. Thomas Hearn, Prof. Shunping Pei, the Editor Prof. Martha Savage, and the associate editor for their helpful comments. This research is supported by the National Natural Science Foundation of China (Grants 41874066, 41674066, 41630210, 41774065, and 41674060). All funding from each author pertaining to this work. There is no conflict of interest for any author from their affiliations or funding.

References

Asamori, K., & Zhao, D. (2015). Teleseismic shear wave tomography of the Japan subduction zone. *Geophysical Journal International*, *203*, 1752–1772. https://doi.org/10.1093/gji/ggv334

Azuma, R., Hino, R., Ohta, Y., Ito, Y., Mochizuki, K., Uehira, K., et al. (2018). Along-arc heterogeneity of the seismic structure around a large coseismic shallow slip area of the 2011 Tohoku-Oki earthquake: 2-D Vp structural estimation through an air gun-ocean bottom seismometer experiment in the Japan Trench Subduction Zone. *Journal of Geophysical Research: Solid Earth*, *123*, 5249–5264. https://doi.org/10.1029/2017JB015361

Cai, C., Wiens, D. A., Shen, W., & Eimer, M. (2018). Water input into the Mariana subduction zone estimated from ocean-bottom seismic data. *Nature*, *563*(7731), 389–392. https://doi.org/10.1038/s41586-018-0655-4

Data Management Centre of China National Seismic Network (2007). Catalog data of China National Seismic Network. Institute of Geophysics, China Earthquake Administration. https://doi.org/10.11998/SeisDmc/SN

Fouch, M. J., Fischer, K. M., Parmentier, E. M., Wysession, M. E., & Clarke, T. J. (2000). Shear wave splitting, continental keels, and patterns of mantle flow. *Journal of Geophysical Research*, *105*(B3), 6255–6275. https://doi.org/10.1029/1999JB900372

Fukao, Y., Obayashi, M., Inoue, H., & Nenbai, M. (1992). Subducting slabs stagnant in the mantle transition zone. *Journal of Geophysical Research*, *97*(B4), 4809–4822. https://doi.org/10.1029/91JB02749

Guo, Z., Chen, Y., Ning, J., Yang, Y., Afonso, J. C., & Tang, Y. (2016). Seismic evidence of on-going sublithosphere upper mantle convection for intra-plate volcanism in Northeast China. *Earth and Planetary Science Letters*, *433*, 31–43. https://doi.org/10.1016/j.epsl.2015.09.035

Hearn, T. M. (1984). Pn travel times in southern California. *Journal of Geophysical Research*, *89*(B3), 1843–1855. https://doi.org/10.1029/JB089iB03p01843

Hearn, T. M. (1996). Anisotropic Pn tomography in the western United States. *Journal of Geophysical Research*, *101*(B4), 8403–8414. https://doi.org/10.1029/96JB00114

Hearn, T. M. (1999). Uppermost mantle velocities and anisotropy beneath Europe. *Journal of Geophysical Research*, *104*(B7), 15,123–15,139. https://doi.org/10.1029/1998JB900088

Hearn, T. M., Wang, S., Ni, J. F., Xu, Z., Yu, Y., & Zhang, X. (2004). Uppermost mantle velocities beneath China and surrounding regions. *Journal of Geophysical Research*, *109*, B11301. https://doi.org/10.1029/2003JB002874

Hirata, N., Karp, B. Y., Yamaguchi, T., Kanazawa, T., Suyehiro, K., Kasahara, J., et al. (1992). Oceanic crust in the Japan Basin of the Japan Sea by the 1990 Japan-USSR expedition. *Geophysical Research Letters*, *19*(20), 2027–2030. https://doi.org/10.1029/92GL02094

Horne, A. V., Sato, H., & Ishiyama, T. (2017). Evolution of the Sea of Japan back-arc and some unsolved issues. *Tectonophysics*, *710*, 6–20. https://doi.org/10.1016/j.tecto.2016.08.020

Hu, J., Faccenda, M., & Liu, L. (2017). Subduction-controlled mantle flow and seismic anisotropy in South America. *Earth and Planetary Science Letters*, *470*, 13–24. https://doi.org/10.1016/j.epsl.2017.04.027

Huang, J., & Zhao, D. (2006). High-resolution mantle tomography of China and surrounding regions. *Journal of Geophysical Research*, *111*, B09305. https://doi.org/10.1029/2005JB004066

Huang, Z., Wang, P., Zhao, D., Wang, L., & Xu, M. (2014). Three-dimensional P wave azimuthal anisotropy in the lithosphere beneath China. *Journal of Geophysical Research: Solid Earth*, *119*, 5686–5712. https://doi.org/10.1002/2014JB010963

Huang, Z., Zhao, D., & Liu, X. (2015). On the trade-off between seismic anisotropy and heterogeneity: Numerical simulations and application to Northeast Japan. *Journal of Geophysical Research: Solid Earth*, *120*, 3255–3277. https://doi.org/10.1002/2014JB011784

Iidaka, T., Iwasaki, T., Takeda, T., Moriya, T., Kumakawa, I., Kurashimo, E., et al. (2003). Configuration of subducting Philippine Sea plate and crustal structure in the central Japan region. *Geophysical Research Letters*, *30*(5), 1219. https://doi.org/10.1029/2002GL016517

International Seismological Centre, On-line Bulletin (2016). http://www.isc.ac.uk, Internatl. Seismol. Cent., Thatcham, United Kingdom. https://doi.org/10.31905/D808B830

Iwasaki, T., Kato, W., Moriya, T., Hasemi, A., Umino, N., Okada, T., et al. (2001). Extensional structure in northern Honshu Arc as inferred from seismic refraction/wide-angle reflection profiling. *Geophysical Research Letters*, *28*(12), 2329–2332. https://doi.org/10.1029/2000GL012783

Jolivet, L., Tamaki, K., & Fournier, M. (1994). Japan Sea, opening history and mechanism: A synthesis. *Journal of Geophysical Research*, *99*(B11), 22,237–22,259. https://doi.org/10.1029/93JB03463

Kaminski, E., & Ribe, N. M. (2001). A kinematic model for recrystallization and texture development in olivine polycrystals. *Earth and Planetary Science Letters*, *189*(3–4), 253–267. https://doi.org/10.1016/S0012-821X(01)00356-9

Karato, S., & Jung, H. (1998). Water, partial melting and the origin of the seismic low velocity and high attenuation zone in the upper mantle. *Earth and Planetary Science Letters*, *157*(3-4), 193–207. https://doi.org/10.1016/S0012-821X(98)00034-X

Kodaira, S., Takahashi, N., Park, J., Mochizuki, K., Shinohara, M., & Kimura, S. (2000). Western Nankai Trough seismogenic zone: Results from a wide-angle ocean bottom seismic survey. *Journal of Geophysical Research*, *105*(B3), 5887–5905. https://doi.org/10.1029/1999JB900394

Laske, G., Masters, G., Ma, Z., & Pasyanos, M. (2013). Update on CRUST1.0 – A 1-degree Global Model of Earth's Crust. *Geophysical Research Abstracts*, *15*.

Legendre, C. P., Zhao, L., & Chen, Q. (2015). Upper-mantle shear-wave structure under East and Southeast Asia from Automated Multimode Inversion of waveforms. *Geophysical Journal International*, *203*(1), 707–719. https://doi.org/10.1093/gji/ggv322

Lei, J., & Zhao, D. (2005). P-wave tomography and origin of the Changbai intraplate volcano in Northwest Pacific. *Tectonophysics*, *397*(3-4), 281–295. https://doi.org/10.1016/j.tecto.2004.12.009

Li, C., van der Hilst, R. D., Engdahl, E. R., & Burdick, S. (2008). A new global model for P wave speed variations in Earth's mantle. *Geochemistry Geophysics Geosystems*, *9*, Q05018. https://doi.org/10.1029/2007GC001806

Li, J., Wang, X., Wang, X. D., & Yuen, A. (2013). P and SH velocity structure in the upper mantle beneath Northeast China: Evidence for a stagnant slab in hydrous mantle transition zone. *Earth and Planetary Science Letters*, *367*, 71–81. https://doi.org/10.1016/j.epsl.2013.02.026

Li, S., Guo, Z., & Chen, Y. J. (2017). Complicated 3D mantle flow beneath Northeast China from shear wave splitting and its implication for the Cenozoic intraplate volcanism. *Tectonophysics*, *709*, 1–8. https://doi.org/10.1016/j.tecto.2017.04.015

Li, X., Song, X., & Li, J. (2017). Pn tomography of South China Sea, Taiwan Island. Philippine archipelago. adjacent regions. *Journal of Geophysical Research: Solid Earth*, *122*, 1350–1366. https://doi.org/10.1002/2016JB013787

Li, Y., Wu, Q., Pan, J., & Sun, L. (2012). S-wave velocity structure of Northeast China from joint inversion of Rayleigh wave phase and group velocities. *Geophysical Journal International*, *190*(1), 105–115. https://doi.org/10.1111/j.1365-246X.2012.05503.x

Liu, X., & Zhao, D. (2016). P and S wave tomography of Japan subduction zone from joint inversions of local and teleseismic travel times and surface-wave data. *Physics of the Earth and Planetary Interiors*, *252*, 1–22. https://doi.org/10.1016/j.pepi.2016.01.002

Liu, Y., Niu, F., Chen, M., & Yang, W. (2017). 3-D crustal and uppermost mantle structure beneath NE China revealed by ambient noise adjoint tomography. *Earth and Planetary Science Letters*, *461*, 20–29. https://doi.org/10.1016/j.epsl.2016.12.029

Long, M. D. (2013). Constraints on subduction geodynamics from seismic anisotropy. *Reviews of Geophysics*, *51*, 76–112. https://doi.org/10.1002/rog.20008

Long, M. D., & van der Hilst, R. D. (2005). Upper mantle anisotropy beneath Japan from shear wave splitting. *Physics of the Earth and Planetary Interiors*, *151*(3-4), 206–222. https://doi.org/10.1016/j.pepi.2005.03.003

Lü, Y., Liu, B., Pei, S., Sun, Y., Toksöz, M. N., & Zeng, X. (2012). Pn tomographic velocity and anisotropy beneath the Iran region. *Bulletin of the Seismological Society of America*, *102*(1), 426–435. https://doi.org/10.1785/0120100141

Lü, Y., Ni, S., Chen, L., & Chen, Q.-F. (2017). Pn tomography with Moho depth correction from eastern Europe to western China. *Journal of Geophysical Research: Solid Earth*, *122*, 1284–1301. https://doi.org/10.1002/2016JB013052

Metcalfe, I. (2006). Palaeozoic and Mesozoic tectonic evolution and palaeogeography of East Asian crustal fragments: the Korean Peninsula in context. *Gondwana Research*, *9*(1-2), 24–46. https://doi.org/10.1016/j.gr.2005.04.002

Nakajima, J., & Hasegawa, A. (2004). Shear-wave polarization anisotropy and subduction-induced flow in the mantle wedge of northeastern Japan. *Earth and Planetary Science Letters*, *225*(3-4), 365–377. https://doi.org/10.1016/j.epsl.2004.06.011

Nakajima, J., Shimizu, J., Hori, S., & Hasegawa, A. (2006). Shear-wave splitting beneath the southwestern Kurile arc and northeastern Japan arc: A new insight into mantle return flow. *Geophysical Research Letters*, *33*, L05305. https://doi.org/10.1029/2005GL025053

Nishimura, C. E., & Forsyth, D. W. (1989). The anisotropic structure of the upper mantle in the Pacific. *Geophysical Journal International*, *96*(2), 203–229. https://doi.org/10.1111/j.1365-246X.1989.tb04446.x

Niu, X., Zhao, D., Li, J., & Ruan, A. (2016). P wave azimuthal and radial anisotropy of the Hokkaido subduction zone. *Journal of Geophysical Research: Solid Earth*, *121*, 2636–2660. https://doi.org/10.1002/2015JB012651

Northrup, C., Royden, L., & Burchfiel, B. (1995). Motion of the Pacific plate relative to Eurasia and its potential relation to Cenozoic extension along the eastern margin of Eurasia. *Geology*, *23*(8), 719–722. https://doi.org/10.1130/0091-7613(1995)023<0719:MOTPPR>2.3.CO;2

Paige, C., & Saunders, M. (1982). LSQR: An algorithm for sparse linear equations and sparse least squares. *ACM Transactions on Mathematical Software*, *8*(1), 43–71. https://doi.org/10.1145/355984.355989

Pandey, S., Yuan, X., Debayle, E., Priestley, K., Kind, R., Tilmann, F., & Li, X. (2014). A 3D shear-wave velocity model of the upper mantle beneath China and the surrounding areas. *Tectonophysics*, *633*, 193–210. https://doi.org/10.1016/j.tecto.2014.07.011

Pei, S., Sun, Y., & Toksöz, M. N. (2011). Tomographic Pn and Sn velocity beneath the continental collision zone from Alps to Himalaya. *Journal of Geophysical Research*, *116*, B10311. https://doi.org/10.1029/2010JB007845

Pei, S., Zhao, J., Sun, Y., Xu, Z., Wang, S., Liu, H., et al. (2007). Upper mantle seismic velocities and anisotropy in China determined through Pn and Sn tomography. *Journal of Geophysical Research*, *112*, B05312. https://doi.org/10.1029/2006JB004409

Ren, J., Tamaki, K., Li, S., & Zhang, J. (2002). Late Mesozoic and Cenozoic rifting and its dynamic setting in eastern China and adjacent areas. *Tectonophysics*, *344*(3-4), 175–205. https://doi.org/10.1016/S0040-1951(01)00271-2

Ribe, N. (1992). On the relation between seismic anosotropy and finite strain. *Journal of Geophysical Research*, *97*(B6), 8737–8747. https://doi.org/10.1029/92JB00551

Schaeffer, A. J., & Lebedev, S. (2013). Global shear speed structure of the upper mantle and transition zone. *Geophysical Journal International*, *194*(1), 417–449. https://doi.org/10.1093/gji/ggt095

Shen, W., Ritzwoller, M. H., Kang, D., Kim, Y., Lin, F. C., Ning, J., et al. (2016). A seismic reference model for the crust and uppermost mantle beneath China from surface wave dispersion. *Geophysical Journal International*, *206*(2), 954–979. https://doi.org/10.1093/gji/ggw175

Sun, W., & Kennett, B. L. N. (2016). Uppermost mantle structure beneath eastern China and its surroundings from Pn and Sn tomography. *Geophysical Research Letters*, *43*, 3143–3149. https://doi.org/10.1002/2016GL068618

Takeuchi, N., Kawakatsu, H., Tanaka, S., Obayashi, M., Chen, Y. J., Ning, J., et al. (2014). Upper mantle tomography in the northwestern Pacific region using triplicated P waves. *Journal of Geophysical Research: Solid Earth*, *119*, 7667–7685. https://doi.org/10.1002/2014JB011161

Tang, Y., Obayashi, M., Niu, F., Grand, S. P., Chen, Y. J., Kawakatsu, H., et al. (2014). Changbaishan volcanism in northeast China linked to subduction-induced mantle upwelling. *Nature Geoscience*, *7*(6), 470–475. https://doi.org/10.1038/ngeo2166

Wang, J., & Zhao, D. (2013). P-wave tomography for 3-D radial and azimuthal anisotropy of Tohoku and Kyushu subduction zones. *Geophysical Journal International*, *193*(3), 1166–1181. https://doi.org/10.1093/gji/ggt086

Wang, Q., Hao, T., & Jiang, W. (1999). Gravity field and deep structure in Japan Sea. *Progress in Geophysics* (*in Chinese)*, *14*(3), 9–16.

Wang, S., Niu, F., & Zhang, G. (2013). Velocity structure of the uppermost mantle beneath East Asia from Pn tomography and its dynamic implications. *Journal of Geophysical Research: Solid Earth*, *118*, 290–301. https://doi.org/10.1002/jgrb.50085

Watts, A. B., & Bodine, J. H. (1978). A Geophysical atlas of the East and Southeast Asian seas. Free Gravity Field. Geological Society of America, MC-25.

Wei, W., Zhao, D., Xu, J., Wei, F., & Liu, G. (2015). P and S wave tomography and anisotropy in Northwest Pacific and East Asia: Constraints on stagnant slab and intraplate volcanism. *Journal of Geophysical Research: Solid Earth*, *120*, 1642–1666. https://doi.org/10.1002/2014JB011254

Wessel, P., Smith, W., Scharroo, R., Luis, J., & Wobbe, F. (2013). Generic mapping tools: Improved version released. *Eos, Transactions American Geophysical Union*, *94*(45), 409–410. https://doi.org/10.1002/2013EO450001

Xin, H., Zhang, H., Kang, M., He, R., Gao, L., & Gao, J. (2018). High-resolution lithospheric velocity structure of continental China by double-difference seismic travel-time tomography. *Seismological Research Letters*, *90*(1), 229–241. https://doi.org/10.1785/0220180209

Xu, J., Ben-Avraham, Z., Kelty, T., & Yu, H. (2014). Origin of marginal basins of the NW Pacific and their plate tectonic reconstructions. *Earth-Science Reviews*, *130*, 154–196. https://doi.org/10.1016/j.earscirev.2013.10.002

Yao, H., Gouedard, P., Collins, J., McGuire, J., & van der Hilst, R. D. (2011). Structure of young East Pacific Rise lithosphere from ambient noise correlation analysis of fundamental- and higher-mode Scholte-Rayleigh waves. *Comptes Rendus Geoscience*, *343*(8-9), 571–583. https://doi.org/10.1016/j.crte.2011.04.004

Yoon, S. H., Sohn, Y. K., & Chough, S. K. (2014). Tectonic, sedimentary, and volcanic evolution of a back-arc basin in the East Sea (Sea of Japan). *Marine Geology*, *352*, 70–88. https://doi.org/10.1016/j.margeo.2014.03.004

Zhang, F., Wu, Q., & Li, Y. (2013). A traveltime tomography study by teleseismic P wave data in the Northeast China area. *Chinese Journal of Geophysics (in Chinese)*, *56*(8), 2690–2700.

Zhang, H., Wang, F., Myhill, R., & Guo, H. (2019). Slab morphology and deformation beneath Izu-Bonin. *Nature Communications*, *10*(1), 1310. https://doi.org/10.1038/s41467-019-09279-7

Zhang, S., & Karato, S. (1995). Lattice preferred orientation of olivine aggregates deformed in simple shear. *Nature*, *375*(6534), 774–777. https://doi.org/10.1038/375774a0

Zhao, D. (2017). Big mantle wedge, anisotropy, slabs and earthquakes beneath the Japan Sea. *Physics of the Earth and Planetary Interiors*, *270*, 9–28. https://doi.org/10.1016/j.pepi.2017.06.009

Zhao, D., Yamamoto, Y., & Yanada, T. (2013). Global mantle heterogeneity and its influence on teleseismic regional tomography. *Gondwana Research*, *23*(2), 595–616. https://doi.org/10.1016/j.gr.2012.08.004

Zhao, D., Yanada, T., Hasegawa, A., Umino, N., & Wei, W. (2012). Imaging the subducting slabs and mantle upwelling under the Japan Islands. *Geophysical Journal International*, *190*(2), 816–828. https://doi.org/10.1111/j.1365-246X.2012.05550.x

Zhao, D., Yu, S., & Liu, X. (2016). Seismic anisotropy tomography: New insight into subduction dynamics. *Gondwana Research*, *33*, 24–43. https://doi.org/10.1016/j.gr.2015.05.008

Zhao, L., Allen, R. M., Zheng, T., & Zhu, R. (2012). High-resolution body wave tomography models of the upper mantle beneath Eastern China and the adjacent areas. *Geochemistry Geophysics Geosystems*, *13*, Q06007. https://doi.org/10.1029/2012GC004119

Zhao, L., Xie, X., Tian, B., Chen, Q., Hao, T., & Yao, Z. (2015). Pn wave geometrical spreading and attenuation in Northeast China and the Korean Peninsula constrained by observations from North Korean nuclear explosions. *Journal of Geophysical Research: Solid Earth*, *120*, 7558–7571. https://doi.org/10.1002/2015JB012205

Zheng, Y., Shen, W., Zhou, L., Yang, Y., Xie, Z., & Ritzwoller, M. H. (2011). Crust and uppermost mantle beneath the North China Craton, Northeast China, and the Japan Sea from ambient noise tomography. *Journal of Geophysical Research*, *116*, B12312. https://doi.org/10.1029/2011JB008637

Zhou, Y., Nolet, G., Dahlen, F. A., & Laske, G. (2006). Global upper-mantle structure from finite-frequency surface-wave tomography. *Journal of Geophysical Research*, *111*, B04304. https://doi.org/10.1029/2005JB003677

Zhou, Z., & Lei, J. (2016). Pn anisotropic tomography and mantle dynamics beneath China. *Physics of the Earth and Planetary Interiors*, *257*, 193–204. https://doi.org/10.1016/j.pepi.2016.06.005